Artificial Neural Network Based Adaptive Control of Single Phase Dual Active Bridge With Finite Time Disturbance Compensation

ZAHEER FAROOQ[1], **TAIMUR ZAMAN**[1], **MUHAMMAD AMIR KHAN**[1],
NASIMULLAH[1], **(Member, IEEE), S. M. MUYEEN**[2], **(Senior Member, IEEE),**
AND ASIER IBEAS[3]

[1]Department of Electrical Engineering, CECOS University of IT and Emerging Sciences, Peshawar 25124, Pakistan
[2]School of Electrical Engineering Computing and Mathematical Sciences, Curtin University, Perth, WA 6102, Australia
[3]Department of Telecommunications and Systems Engineering, Escola d'Enginyeria, Autonomous University of Barcelona, 08193 Barcelona, Spain

Corresponding author: Nasimullah (nasimullah@cecos.edu.pk)

ABSTRACT Single phase Dual Active Bridge (DAB) has found numerous applications in modern energy architectures such as direct current (DC) microgrid, electrical vehicle charging and high voltage direct current (HVDC) system. Due to the model complexities of DAB, this work proposes a model free adaptive control method based on artificial neural network (AANN) which is capable of adjusting the weights online in finite time. The finite time learning property of the proposed controller makes it perfectly robust for the compensation of the disturbances due to source and load side variations. A proportional integral (PI) controller is used to stabilize the nominal dynamics of the system along with the AANN controller. The structure of the proposed controller is as simple as PID controller and as robust as any nonlinear control method. The AANN-PI controller is implemented on TI Launchpad (TMS320F28379D) with a 50 Watts laboratory scale DAB test bench. Finally, the performance of the AANN-PI method is compared experimentally with classical PI and sliding mode controllers.

INDEX TERMS Artificial neural network, control system, dual active bridge, dc-dc converters.

I. INTRODUCTION

The abundant utilization of fossil fuels such as coal, oils and natural gases for energy generation has caused enormous pollution problems. In order to meet the future energy demands of the human beings, alternative and clean energy sources have been explored such as wind, solar and geothermal etc. Therefore, trend of traditional utilization of energy is converting to the renewable energy and resources. The renewable energy sources have intermittent nature so these sources are integrated to ac and dc grids through power converters. Moreover, when the power from the renewable energy sources is not at its peak, then energy storage systems are utilized to ensure smooth power to the consumers. In order to enable the bidirectional power flow between the energy storage and the microgrid, dual active bridge is utilized [1], [2]. In addition to the above, the rise in environmental pollution is compelling the global manufacturers to develop electrical

vehicles (EV) [3]. The key element of energy transferring in electric vehicles is the bidirectional DC/DC converter. With such enormous applications, the research and development in the bidirectional DC/DC converters is more valuable [4]. A thematic concept of smart grid is shown in Fig. 1.

A. LITERATURE BACKGROUND

An extensive expendability of the DC-DC converters in smart grids has attracted the attention of researchers towards new topology developments, converter's stability and its high control performance. Due to the intermittent nature of the renewable energy resources, it is common to integrate energy storage system in the modern architecture of the microgrid. The bidirectional power flow is achieved by utilizing the bidirectional DC-DC converters alternatively called as dual active bridge (DAB) converters. DAB converter is connected between the energy storage system and the DC bus. In the event, when the renewable energy sources have surplus energy so the DAB is utilized to extract energy from the

---

The associate editor coordinating the review of this article and approving it for publication was Yanzheng Zhu.

IEEE *Access*

Z. Farooq *et al.*: Artificial Neural Network Based Adaptive Control of Single Phase DAB With Finite Time Disturbance Compensation
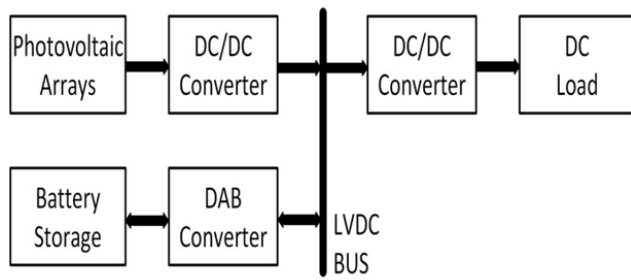
FIGURE 1. Ideal DC microgrid configuration.

DC bus and use it for charging the energy storage and vice versa [5], [6].

Lot of literature is available about the topologies of the DAB converters. However due to intrinsic behavior of these converters for special applications and their topologies, they are divided into isolated and non-isolated bidirectional converters [10]. The non-isolated converters are operated in buck, boost or buck-boost mode where it can be utilized for unidirectional power flow applications. Besides non-isolated converters, the fly-back converter, half H-bridge converter, push-pull and full H-bridge converters are characterized as bidirectional isolated converters. The isolated bidirectional H-bridge converters are more convenient to use in applications like microgrid, un-interruptable power supplies and specifically V2G interface etc. To operate the isolated bidirectional dual active bridge (IBDAB), different modulation techniques are reported by researchers in literature [11]–[13].

Among different modulation techniques, conventional single phase shift (SPS) based modulation technique is very easy to implement. In SPS method a single variable δ is used as a phase shift angle between the primary and secondary bridge of IBDAB to control the flow of power. To implement SPS, one degree of freedom variable is required. SPS has some inherent disadvantages such as the existence of circulating currents, zero voltage switching for a low range of the total period and losses. A two and three degree of freedom modulation topology called dual phase shift (DPS) and triple phase shift (TPS) methods have been reported in [14], [15]. Although the DPS and TPS methods show more advantages as compared to the SPS; however, these methods are more complex to implement. Moreover, the complex control system is required to generate more control variables. As an example, the DPS method requires two control variables to control the power flow i.e. phase shift angles δ_d and δ_s. δ_d is the phase shift angle incorporated between the complementary switches of the primary bridge; whereas, the outer phase shift δs corresponds to the phase angle between the primary and secondary side bridges of IBDAB.

The closed loop DAB performance and stability depends on feedback control system. Different literature has been reported regarding the closed loop control of bidirectional dual active bridge. A robust control system for DAB leads to a stable bus voltage, good battery management and overall fast

dynamic systems response. In [16]–[18], the conventional PI controllers are reported for bidirectional dual active bridge. However uncertainties and variations in system dynamics can cause instability and poor performance of the controller. In [19], a flatness based controller is proposed for DAB converter however the controller structure is more similar to PID. In [20], a fuzzy logic system based control scheme is proposed for dual active bridge. The proposed controller is fixed and so it is not robust against the source and load side variations. In [21], a predictive phase shift control method is proposed. A hybrid controller based on ant clone and BP neural network method has been reported in [15]. Similarly in [22], [28], [29], a fixed weights neural controller is reported to control the power flow between a source and a hybrid vehicle. The reported controller in [15] is a type of fixed controller and will take more resources when implemented on processor. In [23], [24], robust sliding mode controllers are proposed based on the dynamic model of the DAB. The derived model is based on the 1st harmonic of the Fourier series of the square wave and neglects the other harmonic states. In addition, [23], [24] replaces the signum function by a continuous approximation i.e. *tanh* so the robustness of the control system is compromised.

B. MOTIVATION AND INNOVATION

The aim of this study is to design a close loop control for high high voltage tracking side of DAB. The closed loop control is developed by combination of the proportional-integral (PI) control and single neuron adaptive control (AANN) system. The PI controller is used as a base controller and it stabilizes the nominal dynamics of the DAB converter. With source and load variations, PI controller is not robust enough so the AANN controller is used for the compensation of the disturbance terms induced as a result of the mentioned variations. Weights of the proposed control system are tuned online using Hebbian algorithm [25]. The proposed control system is easy to implement as it doesn't need complex system modeling and exhibits robustness to source and load variations. Moreover, due to the finite time adaptation of the weights, the proposed controller compensates for the variations in finite time.
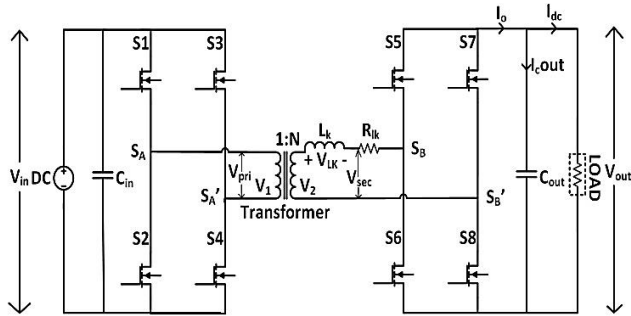
C. ORGANIZATION

This paper is organized as following. In Section 2, the basic configuration and waveforms of bidirectional dual active bridge using SPS are explained. In section 3, the mathematical modeling of the converter is derived. Closed loop control and basic derivations are included in section 4. The experimental results are discussed in section 5. In the last section the research is concluded.

II. THE DUAL ACTIVE BRIDGE DC/DC CONVERTER
A. BASIC PRINCIPLE AND OPERATIONS
The general block diagram considered for this study is shown in Fig. 2. The IBDAB converter consists of switching devices (S_1-S_8), with a high frequency transformer connected

Z. Farooq et al.: Artificial Neural Network Based Adaptive Control of Single Phase DAB With Finite Time Disturbance Compensation

IEEE Access

FIGURE 2. Circuit configuration of bidirectional dual active bridge converter.

FIGURE 3. Single phase shift (SPS) modulation operating waveforms.

in between the two bridges. The two bridges are connected at the primary and secondary sides of the transformer such that one acts as input bridge (on primary side) and the other as output bridge (on secondary side), respectively. Whereas, the transformer provides the galvanic isolation between the two bridges and also serves as a power transferring element in addition with leakage inductor L_k connected in series. For this study, the IBDAB is connected to variable power supply (V_{in}) (varying between 14-24 volts) and variable load. The variable load is switched with fast relay modules operated through microcontroller. Due to symmetry of IBDAD topology, the output voltage is controlled only. The proposed control is implemented using SPS method. The switching devices (S_1-S_8) are operated with fixed 50 percent duty cycle. The phase shift φ between the primary and secondary H-bridges determines the amount of power to be transferred. Considering loss less high frequency transformer, the power can be transferred from primary to secondary side using (1) [23].

$$P_O = \frac{V_{in}V_{out}}{2Nf_sL_k}d\,(1-d) \tag{1}$$

where, L_k is the leakage inductance of the inductor, f_s is the switching frequency and N represents the turn ratio of the transformer. In addition, d $= \delta/\pi$ is the phase shift ratio; V_{in} and V_{out} are the input and output voltages, respectively.

B. GENERAL WAVEFORM OPERATION

In order to transfer power from the low voltage to high voltage side, the bridge at the primary side is operated with leading phase shift with respect to the bridge at secondary side. Fig. 3 shows the operating waveform when power is transferred from the primary (V_{pri}) to secondary (V_{sec}) side.

III. MATHEMATICAL MODELING

In this section, detailed mathematical model for DAB converter is derived which is based on first harmonic of the Fourier series of the square wave. Fig. 3 explains the basic working of the SPS modulation. In each bridge switches are operated with 50 percent duty cycle with a phase shift δ between the two modulating wave forms. In order to analyze the dynamics of the DAB, accurate mathematical models are
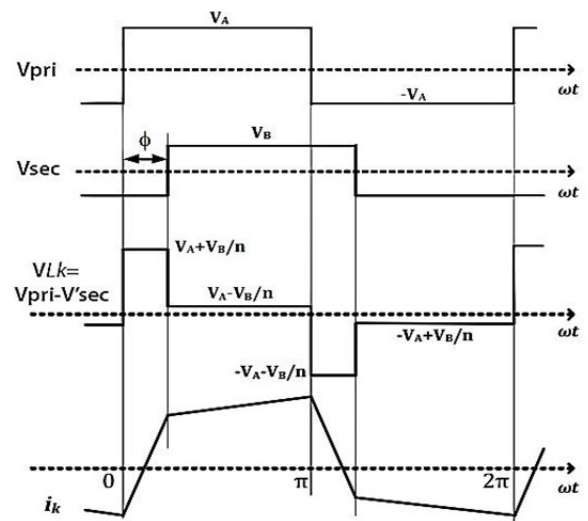
required. The mathematical model is derived by relating the MOSFET's leg switching function into Fourier series with equivalent harmonic representations. The switching functions of leg (A) are given as following [26].

$$S_A = \frac{1}{2} + \frac{2}{\pi}\sum_{n=0}^{\infty} \frac{sin\,(2n+1)\,(\omega_s t)}{2n+1} \tag{2}$$

$$S_A' = S_A\left(t - \frac{\pi}{\omega_s}\right) \tag{3}$$

From Fig. 2, $V_1 = V_{pri}$ and $V_2 = NV_1$, where N is the transformer's turn ratio. The expression for the primary voltage is written as following.

$$V_{pri} = V_{in}\left[S_A - S_A'\right] \tag{4}$$

$$V_{pri} = V_{in}\frac{4}{\pi}\sum_{n=0}^{\infty} \frac{sin\,(2n+1)\,(\omega_s t)}{2n+1} \tag{5}$$

Similarly, the switches of high side bridge are operated with phase delay (δ), so the switching function of leg B with phase delay is expressed as following.

$$S_B = \frac{1}{2} + \frac{2}{\pi}\sum_{n=0}^{\infty} \frac{sin\,(2n+1)\,(\omega_s t - \delta)}{2n+1} \tag{6}$$

The secondary side voltage can be written as,

$$V_{sec} = V_{out}\left[S_B - S_B'\right] \tag{7}$$

$$V_{sec} = V_{out}\frac{4}{\pi}\sum_{n=0}^{\infty} \frac{sin\,(2n+1)\,(\omega_s t - \delta)}{2n+1} \tag{8}$$

The voltage expression for the high voltage side of the transformer is expressed as following,

$$R_k i_{lk}\,(t) + L_k\frac{di_{lk}\,(t)}{dt} = Nv_{pri}\,(t) - V_{sec}\,(t) \tag{9}$$

Here, $N = \frac{N_s}{N_p}$ represents the transformer turn ratio. By putting (5) and (8) in (9), one obtains,

$$N\left[V_{in}\frac{4}{\pi}\sum_{n=0}^{\infty}\frac{sin\,(2n+1)\,(\omega_s t)}{2n+1} \right.$$
$$\left. - V_{out}\frac{4}{\pi}\sum_{n=0}^{\infty}\frac{sin\,(2n+1)\,(\omega_s t-\delta)}{2n+1} \right]$$
$$= R_k i_{lk}\,(t) + L_k\frac{di_{lk}\,(t)}{dt} \tag{10}$$

By re-arranging (10), the expression for i_{lk} is obtained as,

$$i_{lk}\,(t) = \frac{4}{\pi}\sum_{n=0}^{\infty}\frac{1}{(2n+1)}$$
$$\times\left[\begin{array}{c} \frac{NV_{pri}}{|Z\,(n)|}sin\,(2n+1)\,\omega_s t - \varphi_Z\,(n) \\ -\frac{V_{sec}}{|Z\,(n)|}sin\,(2n+1)\,(\omega_s t-\delta) - \varphi_Z\,(n) \end{array} \right] \tag{11}$$

$$|Z\,(n)| = \sqrt{R_{lk}^2 + [(2n+1)\,\omega_s L_k]^2} \tag{12}$$

$$\varphi_Z\,(n) = tan^{-1}\left(\frac{(2n+1)\,\omega_s L_k}{R_{lk}} \right) \tag{13}$$

Here ω_s is the switching frequency, $|Z(n)|$ represents the impedance of the two bridges and $\varphi_z(n)$ is the corresponding phase angle. By applying Kirchhoff's current law (KCL) at the load side node of the DAB converter of Fig. 2, one obtains,

$$I_o = I_{cout} + I_{dc} \tag{14}$$

$$I_{cout} = I_o - I_{dc} \tag{15}$$

By re arranging (15) and including the dynamics of the switching functions, the following expressions are obtained.

$$C\frac{dV_{cout}}{dt} = I_o - I_{dc} \tag{16}$$

$$C\frac{dV_{cout}}{dt} = I_{lk}(S_B - S'_B) - I_{dc} \tag{17}$$

$$C\frac{dV_{cout}}{dt} = I_{lk}(S_B - S'_B) - \frac{V_{cout}}{R_{load}} \tag{18}$$

By combining (11), (7) and (18) one obtains

$$\frac{dV_{cout}\,(t)}{dt}$$
$$= -\frac{V_{cout}\,(t)}{R_{load}}$$
$$+ \frac{1}{C_{out}}\left[\frac{4}{\pi}\sum_{n=0}^{m} \begin{array}{c} \frac{NV_{in}}{(2n+1)|Z\,(n)|}sin\left(\begin{array}{c}(2n+1)\,\omega_s t \\ -\varphi_z\,(n)\end{array} \right) \\ -V_{out}sin\left(\begin{array}{c}(2n+1)\,\omega_s t-\delta \\ -\varphi_z\,(n)\end{array} \right) \end{array} \right]$$
$$+ \frac{4}{\pi}\sum_{r=0}^{1}\frac{1}{(2r+1)}sin\,((2r+1)\,(\omega_s t-\delta)) \tag{19}$$

From [23], (19) can be re written as (20)

$$\frac{dV_{cout}}{dt} = \frac{-8}{C_{out}\pi^2}\sum_{n=1,3,5,..}^{\infty}\frac{cos\,(\varphi_z\,(n))}{n^2\,|Z\,(n)|}V_{out}$$
$$+ \frac{8}{C_{out}\pi^2}\sum_{n=1,3,5,..}^{\infty}\frac{cos\,(n\delta - \varphi_z\,(n))}{n^2\,|Z\,(n)|}NV_{in} - \frac{I_{dc}}{C_{out}} \tag{20}$$

In (20), N represents the turn's ratio of the transformer whereas; n refers to number of harmonic state. By placing $n = 1$ yields the state space model of the DAB based on 1st harmonic of the Fourier series and it is expressed as following.

$$\dot{X} = F\,(x) + G\,(x)\,U + D \tag{21}$$

Here the terms $F(x)$, $G(x)$ and D are defined as following

$$F(x) = \frac{-8}{C_{out}\pi^2}\sum_{n=1,3,5,..}^{\infty}\frac{cos\,(\varphi_z\,(n))}{n^2\,|Z\,(n)|}V_{out},$$

$$G(x) = \frac{8}{C_{out}\pi^2}\sum_{n=1,3,5,..}^{\infty}\frac{1}{n^2\,|Z\,(n)|}NV_{in},$$

$$D = \frac{-8}{C_{out}\pi^2}\sum_{n=3,5,..}^{\infty}\frac{cos\,(\varphi_z\,(n))}{n^2\,|Z\,(n)|}V_{out}$$
$$+ \frac{8}{C_{out}\pi^2}\sum_{n=3,5,..}^{\infty}\frac{cos\,(n\delta - \varphi_z\,(n))}{n^2\,|Z\,(n)|}NV_{in}$$
$$- \frac{I_{dc}}{C_{out}} + d_{load} + d_{source}$$

The lumped disturbance term D contains all the higher order harmonics including the disturbance terms due to source variation d_{source} and the load variation d_{load}. Therefore, (21) does not represent the accurate nominal dynamics of the DAB converter when other harmonics states are not considered.

IV. CLOSE LOOP CONTROL

This section of the paper proposes two controllers. The first controller is based on the ANN, which tunes the gains of the PI controller. The second controller is based on integral sliding mode control. The results of both controllers are compared.

Artificial Neural Networks: The artificial neural networks are composed of billions and trillions of neurons which continuously interact with each other and process the information. The ANN is imitated from biological neural networks and is designed as such that the information taken as input is forwarded through nodes to the output. The output of the ANN networks is similarly called an activation function or node value. Following up the artificial single neuron based method as shown in Fig. 4, the gains of the PI controller are tuned. Where, $x = [x_1 x_2 \ldots x_m]^T$ refers to the number of inputs and $w = [w_0 w_1 \ldots w_m]^T$ denote the weights. Using ANN, Hebb based algorithm is followed to tune the
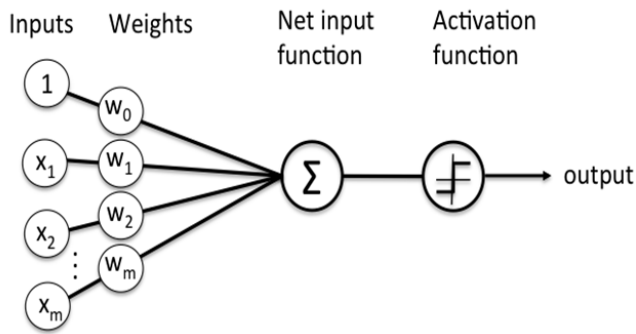
Z. Farooq et al.: Artificial Neural Network Based Adaptive Control of Single Phase DAB With Finite Time Disturbance Compensation

IEEE *Access*

Inputs   Weights   Net input function   Activation function

output

FIGURE 4. Single phase shift (SPS) modulation operating waveforms.

parameters of PI controller, which are briefly discussed in section A.

A. AANN-PI

In this section, the proposed control topology is discussed in details. The dynamic model of (21) is based on first harmonic of Fourier series of the square wave. Moreover, the disturbance term D is very complex. Due to the model complexities, this work proposes a model free adaptive control method which is capable of adjusting the weights online in finite time. The finite time learning property of the proposed controller makes it perfectly robust for the compensation of the disturbances due to source and load side variations. The implementation of the proposed control is shown in Fig. 5. General expression for fixed gain proportional, derivative and integral (PID) is written as following.

$$u_{PID}(k) = K_p e(k) + K_i \sum_{n=1}^{k} e(n) + K_d(e(k) - e(k-1))$$
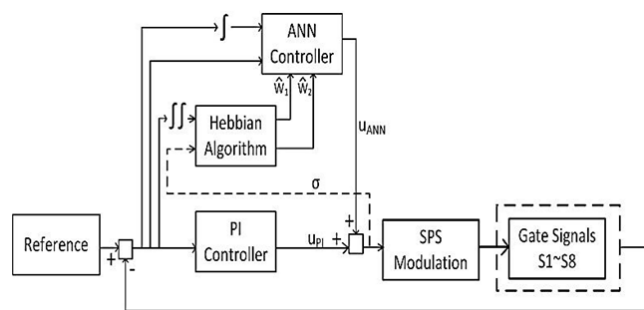
$$(22)$$

FIGURE 5. Block diagram of proposed adaptive artificial neural networks based PI controller.

Here, e represents the error between the reference command and feedback signal, K_P is proportional constant, K_i represents integral gain and K_d is the derivative gain [18]. The classical fixed PID control is not robust to the nonlinear tracking commands, source and load side variations. To overcome this limitation and in order to achieve desired tracking response, an auxiliary controller based on adaptive ANN method is

integrated with the classical PI control. The auxiliary controller is a single neuron controller and its weights are tuned online using Hebbian method. The overall control scheme is mathematically represented as following.

$$u_T(k) = u_{PID}(k) + u_{AANN}(k) \qquad (23)$$

In (23), PID controller is discretized using Tustin method. Moreover, the second term u_{AANN} represents the adaptive control scheme based on ANN method. Mathematically the AANN controller is written as following

$$u_{AANN}(k) = \sum_{i=1}^{i=n} W_i(k) x_i(k) \qquad (24)$$

In (24), W_i represent the weights and x_i is the state vector. By choosing $x_1(k) = e(k), x_2(k) = \sum_{n=1}^{k} e(n) \, for \, i = 1, 2 \dots$ and considering $K_d = 0$ in this case. Using (22) and (23), (24) is modified as following.

$$u_T(k) = \left(\hat{W}_1(k) + K_p\right) x_1(k) + \left(\hat{W}_2(k) + K_i\right) x_2(k) \qquad (25)$$

In (25), $\hat{W}_1$ and $\hat{W}_2$ are the adaptive weights that are tuned online using the following discrete expression of the following form.

$$\hat{W}_i(k) = \left(\hat{W}_i(k-1) + \eta_i z_i(k) u(k)\right) \qquad (26)$$

In (26), $z_i(k) = \sum_{n=1}^{k} \sum_{n=1}^{k} e(n)$, and it represents the double integral of error at k^{th} sample. The $u(k) = \sigma(k)$ corresponds to the kth sample of control signal which is phase shift and η_i represents the learning rates of the adaptive algorithm. In addition, from (26) the upper limits of the gain terms are chosen as $(\hat{W}_1 + K_p) \leq \zeta 1$ and $(\hat{W}_2 + K_i \leq \zeta 2)$. All the parameters used in the proposed controller are tabulated in table 2.

B. INTEGRAL SLIDING MODE CONTROL

In this section, single integral sliding mode control system is derived based on the mathematical model given in (21). Let $e = X - X_d$ represents the voltage tracking error, and $e^\cdot = X^\cdot - X_d^\cdot$ be its first derivative, then the sliding surface is defined as following.

$$S_v = C_1 e + C_2 \int e \qquad (27)$$

Here C_1 and C_2 represent the gain of the sliding surface. Taking first derivative of (27) and combining it with (21) yields the following equation.

$$S_v^\cdot = C_1 F(x) + C_1 D + C_1 G(x) U + C_2 e - X_d^\cdot \qquad (28)$$

$$U = -(C_1 G(x))^{-1} \begin{bmatrix} C_1 F(x) + C_1 D + C_2 e \\ -X_d^\cdot - k_r sgn(S_v) \end{bmatrix} \qquad (29)$$

From (29), the phase shift is implemented as $\delta = \sin^{-1}(U)$ as discussed in [23], [24]. By combining (28), (29) and by letting discontinuous gain $K_r > D_{max}$, it is easy to show that $S_v^\cdot \cong 0$, which shows the reaching condition of the sliding surface.

IEEE *Access*

Z. Farooq *et al.*: Artificial Neural Network Based Adaptive Control of Single Phase DAB With Finite Time Disturbance Compensation

V. RESULTS AND DISCUSSIONS

A. EXPERIMENTAL SETUP AND PARAMETERS

To verify the control algorithm shown in Fig. 5, a laboratory scaled dual active bridge test bench of 150 watts is developed. The proposed control method is tested under the following three conditions: 1. Variable reference command, 2. Source variation 3. Load variation disturbance.

The proposed controller is implemented using rapid proto-typing technique with Simulink interface. The experimental setup is shown in Fig. 6. The parameters of the test bench are tabulated in Table 1 and gains of the controllers are given in Table 2. In addition, the gains of the PI controller are derived for DAB converter using small signal analysis as discussed in [27]. Also, the SMC and ANN gains are determined by trial and error method.
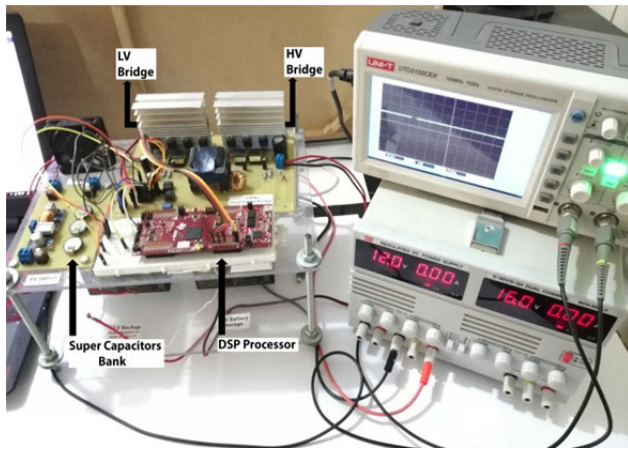

FIGURE 6. Experimental setup of Bidirectional DAB.

TABLE 1. Parameters for experiment.

Parameters	Value
Rated output power	50 watts
Input voltage (Vin)	12V
Output voltage (Vout)	24V
Cin, Cout	100μF, 200μF
N	1:2
L_{sk}	50 μH
Load	100 Ah

B. TEST UNDER VARIABLE REFERENCE COMMAND

1) VOLTAGE TRACKING PERFORMANCE WITH PI CONTROLLER

Fig. 7a shows the voltage tracking performance of DAB with fixed gain PI controller under variable reference command. As shown in Fig. 7a, the reference signal is abruptly changed from 24V to 14V at time t = 20ms, then set back to 24V at time t = 120ms and finally switched back to 14V at time t = 220ms. The parameters of the PI controller are shown in Table 2.

TABLE 2. Control system parameters.

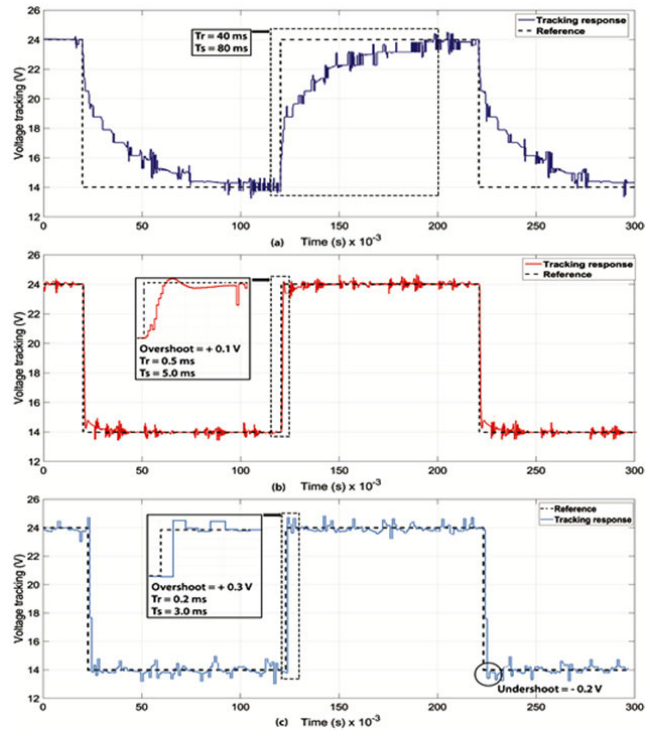| Controller	Parameters	Value
PI	Kp	2.5
	Ki	1.5
AANN-PI	$\hat{W}_1(0)$	0.5
	$\hat{W}_2(0)$	0.5
	η_1	$1e^{-8}$
	η_2	$1.25e^{-8}$
	ζ_1	12
	ζ_1	14
SMC	k_r	100
	C_1	0.05
	C_2	30

FIGURE 7. Voltage tracking performance of DAB under variable reference command for (a) PI controller (b) AANN-PI controller (c) SMC controller.

The output voltage convergence to its reference command with fixed gain PI controller is very poor. Since there is no overshoot while tracking its reference, the controller converges to the reference in 80ms with rise time (T_r) of 40ms. Fig. 8 shows the corresponding change in phase shift. The phase shift is taken as PWM register counts. These ranges in between 0 and 250 counts, which correspond to 0° and 90° of phase shift. Fig. 9 shows the output voltage measured using digital oscilloscope. The voltage tracking performance of fixed gain PI is tabulated in Table 3.
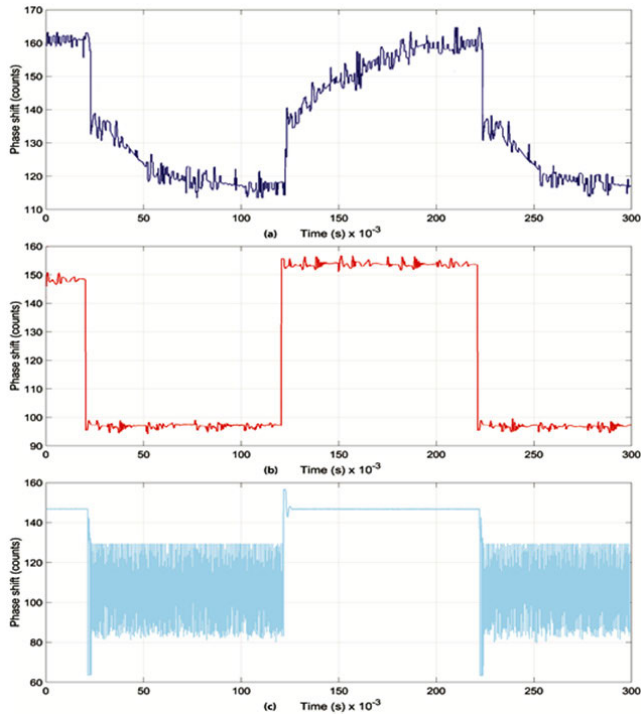
Z. Farooq *et al.*: Artificial Neural Network Based Adaptive Control of Single Phase DAB With Finite Time Disturbance Compensation

IEEE *Access*

FIGURE 8. Phase shift variation under variable reference command for (a) PI controller (b) AANN-PI controller (c) SMC controller.
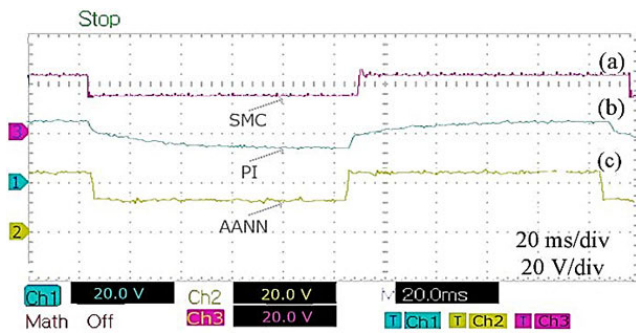

FIGURE 9. Voltage measurement of DAB under variable reference command using digital oscilloscope (a) SMC controller (b) PI controller (c) AANN-PI controller.

2) VOLTAGE TRACKING PERFORMANCE WITH AANN-PI CONTROLLER

The voltage tracking performance of AANN-PI control is shown in Fig. 7b. The proposed controller tracks its reference in finite time with minor overshoot of 0.1V in tracking signal.

The voltage convergence rate of the AANN-PI controller is very fast as compared to the fixed gain PI controller. In addition, settling time of the proposed controller is 5ms with rise time of 0.5ms. Similar results are obtained when the reference voltage is changed back to 14V at 220ms from 24V. Fig. 10 shows the finite time online adaptation of the weights $(\hat{W}_1, \hat{W}_2)$ of the neural network controller with respect to the variations in the reference voltage. The voltage tracking performance of AANN-PI method is tabulated in Table 3. (Due to symmetry table 3 only shows the results tabulated based on one disturbance cycle).

TABLE 3. Comparative analysis.

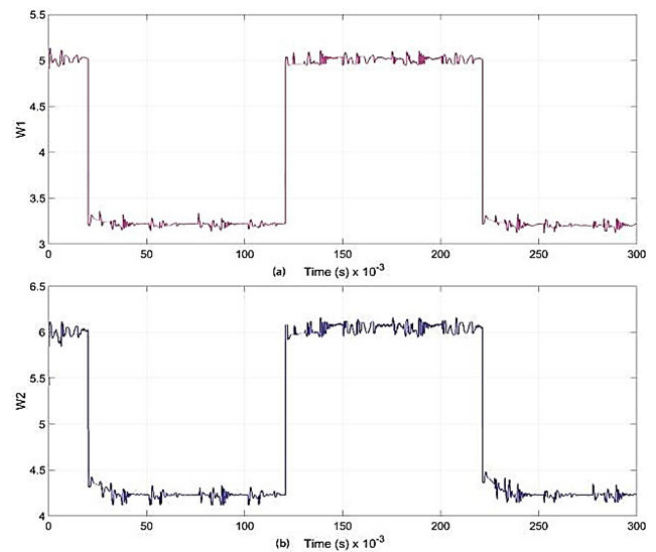| Controller	Response	Reference variation 0<t<300 (ms)	Source variation 0<t<300 (ms)	Load variation 0<t<300 (ms)
PI	Overshoot	0	2.8	2.5
	Undershoot	0	-2.8	-2.3
	Rise time	40	3	4
	Settling time	80	80	80
AANN-PI	Overshoot	0.1	0.9	0.9
	Undershoot	0	-0.8	-0.8
	Rise time	0.5	1.5	2.5
	Settling time	5	9	9
SMC	Overshoot	0.3	0.7	0.7
	Undershoot	-0.2	-0.7	-0.7
	Rise time	0.2	0.2	0.2
	Settling time	3	1	1

FIGURE 10. Online weight tuning of AANN-PI under variable reference command (a) $\hat{w}^1$ (b) $\hat{w}^2$.
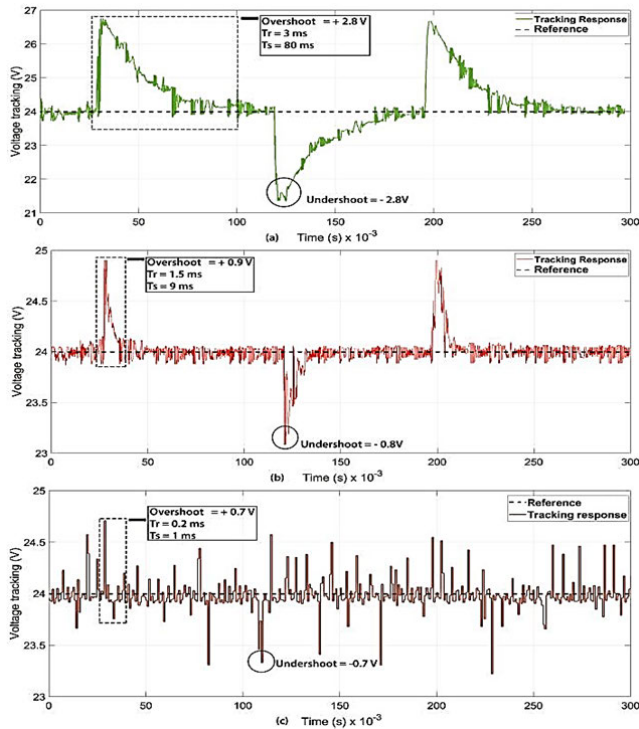
3) VOLTAGE TRACKING PERFORMANCE WITH INTEGRAL SMC CONTROLLER

The voltage tracking performance of integral SMC control is shown in Fig. 7c. The proposed controller tracks its reference in finite time with minor overshoot of 0.3V in tracking the signal. The measured settling and rise times are 3ms and 0.2ms, respectively. Fig. 8c shows the phase shift control signal using the integral SMC control method. From the presented result it is evident the phase shift signal contains high frequency chattering which is not feasible for long period operation of DAB converter. Fig. 9a shows the experimental results collected using digital oscilloscope. (Due to symmetry table 3 only shows the results tabulated based on one disturbance cycle).

C. TEST UNDER VARIABLE SOURCE CONDITION
1) VOLTAGE TRACKING PERFORMANCE WITH PI CONTROLLER

Fig. 11a shows the output voltage regulations with respect to the variations in source voltage. The initial value of source

FIGURE 11. Voltage tracking performance of DAB under variable source voltage (a) PI controller (b) AANN-PI controller (c) SMC controller.
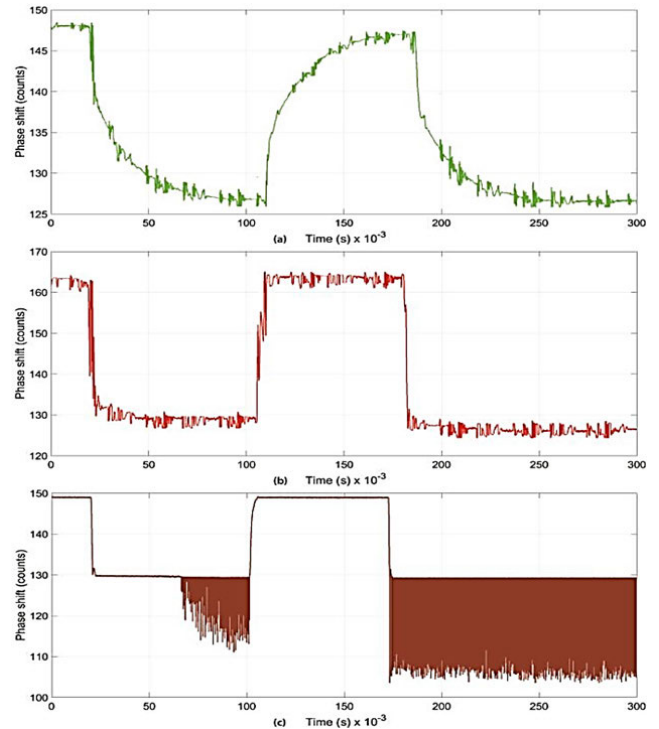

FIGURE 12. Phase shift variation under variable source voltage (a) PI controller (b) AANN-PI controller (c) SMC controller.

voltage is 12V till time t = 20ms. From 120ms onward, the reference voltage is changed to 16V which resulted in an overshoot of 2.8V in the output measured voltage. The output voltage converges slowly to the reference as can be observed in Fig. 11a. The parameters of the test are tabulated in Table 3, which clearly replicate the slow performance of the controller. The corresponding change in the phase shift is shown in Fig. 12a. Fig. 13b shows the experimental results measured using digital oscilloscope.

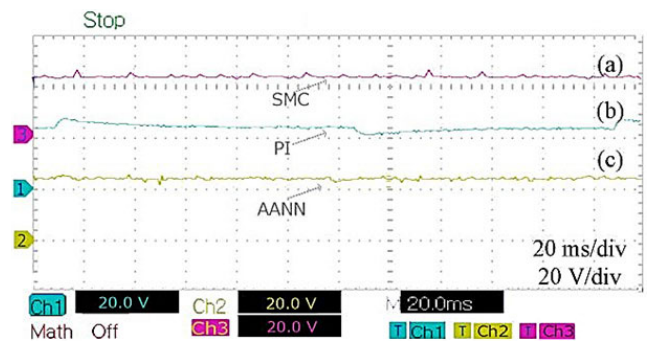### 2) VOLTAGE TRACKING PERFORMANCE WITH ANN-PI CONTROLLER

The voltage tracking performance of AANN-PI controller is given in Fig. 11b. As a result in source variations (as given in subsection V B), the measured overshoot of 0.9V and undershoot of -0.8V in the output voltage are observed. Fig. 13c shows the practical results measured through oscilloscope. Fig.12b shows the measured phase shift and Fig. 14 shows the corresponding online adaptation of the weights ($\hat{W}_1$, $\hat{W}_2$). (Due to symmetry table 3 only shows the results tabulated based on one disturbance cycle).

3) VOLTAGE TRACKING PERFORMANCE WITH SMC CONTROLLER

Fig. 11c shows the output voltage regulations with respect to the variations using SMC control method. From the results it is evident that the SMC Control method is robust to the source variations but the tracking signal contains high frequency oscillations. Due to the high frequency oscillations,

FIGURE 13. Voltage measurement of DAB under variable source voltage using digital oscilloscope for (a) SMC controller (b) PI controller (c) AANN-PI controller.

over shoot of 0.7V and undershoots of −0.7V are observed in the tracking signal. Fig. 12c shows the phase shift response measured and it shows high frequency chattering. Fig. 13a shows the results measured through oscilloscope. (Due to symmetry table 3 only shows the results tabulated based on one disturbance cycle).

D. TEST UNDER VARIABLE LOAD CONDITION

1) VOLTAGE TRACKING PERFORMANCE WITH PI CONTROLLER

Fig. 15a shows the voltage tracking performance of fixed gain PI controller. The undershoot of −2.3V is observed at time t = 120ms when the load is suddenly changed from 200 ohms to 500 ohms. Similarly, an overshoot of 2.5V is observed

Z. Farooq *et al.*: Artificial Neural Network Based Adaptive Control of Single Phase DAB With Finite Time Disturbance Compensation
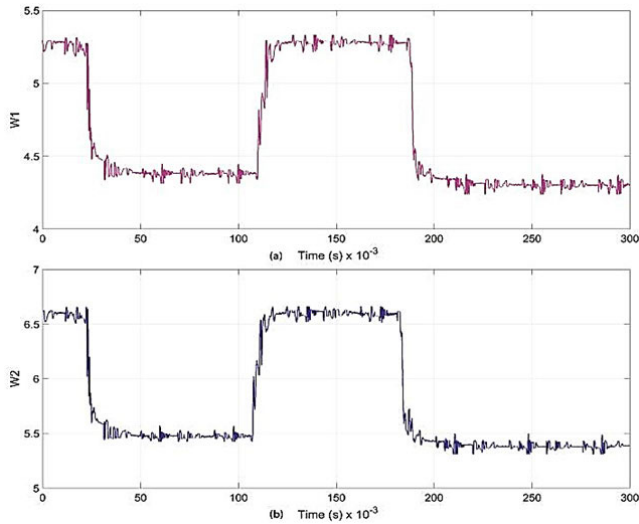
IEEE *Access*

FIGURE 14. Online weight tuning of AANN-PI under variable source voltage a) $\hat{w}_1$ b) $\hat{w}_2$.

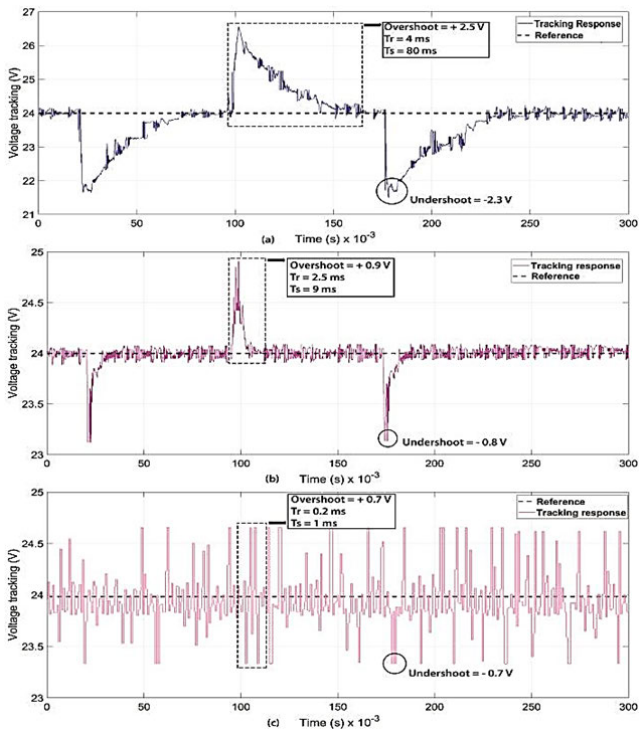**FIGURE 15.** Voltage tracking performance of DAB under load variation for (a) PI controller (b) AANN-PI controller (c) SMC controller.

FIGURE 16. Phase shift variation under load variation for (a) PI controller (b) AANN-PI controller (c) SMC controller.

FIGURE 17. Voltage measurement of DAB under variable load using digital oscilloscope for (a) SMC controller (b) PI controller (c) AANN-PI controller.

at time t = 80ms when the load is restored to 200 ohms. Fig. 17b shows the measured tracking signal using digital oscilloscope. The corresponding phase shift signal is shown in Fig. 16a. Table 3 shows the performance tabulation of the system with fixed gain PI controller under load variations.

2) VOLTAGE TRACKING PERFORMANCE WITH AANN-PI CONTROLLER

Fig. 15b shows the AANN-PI based controller voltage tracking response with finite time adaptation of the weights.
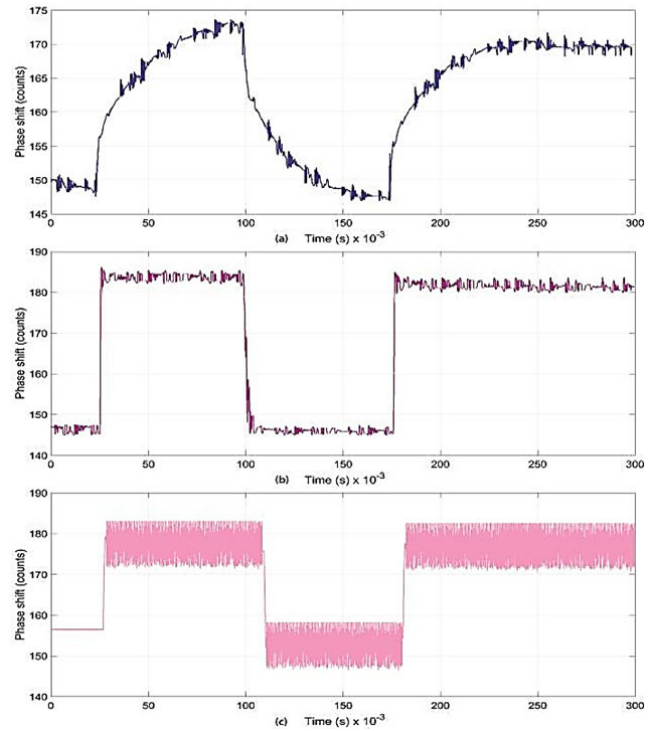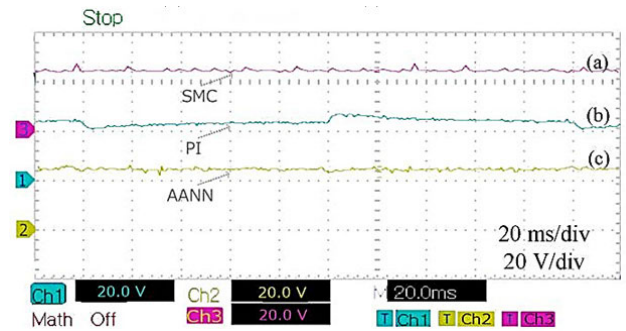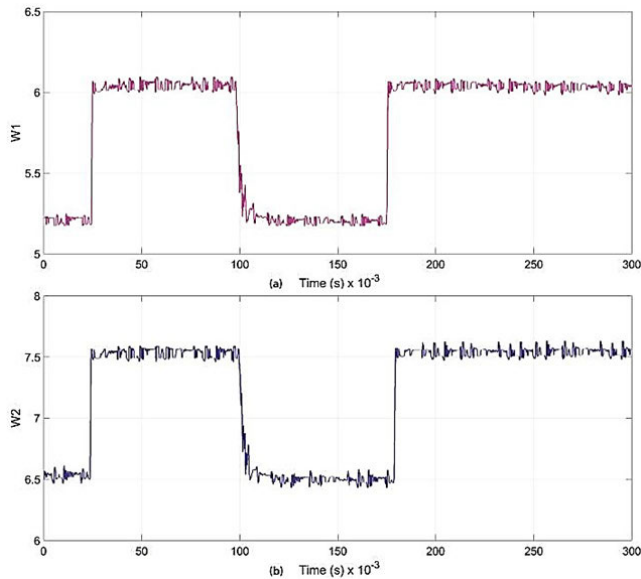
The controller exhibits robustness to the load variations and tracks the desired reference with overall settling time of 9ms. The rise time response of the controller is far better than PI controller which contributes to an accurate and fast reference tracking. Fig. 17c shows the measured voltage signal using digital oscilloscope. The corresponding change in phase shift is shown in Fig. 16b. With finite time disturbance compensation at 20ms, the controller changes the phase shift from 160 to 180 with the online weights adjustments of $\hat{W}_1$ and $\hat{W}_2$ as shown in Fig. 18.

3) VOLTAGE TRACKING PERFORMANCE WITH INTEGRAL SMC CONTROLLER

Fig. 15c shows the output voltage regulations with respect to the variations using SMC control method. From the results

IEEE *Access*

Z. Farooq *et al.*: Artificial Neural Network Based Adaptive Control of Single Phase DAB With Finite Time Disturbance Compensation

FIGURE 18. Online weight tuning of AANN-PI under variable load a) $\hat{w}_1$ b) $\hat{w}_2$.

it is evident that the SMC Control method is robust to the source variations but the tracking signal contains high frequency oscillations. Due to the high frequency oscillations, over shoot of 0.7V and undershoots of -0.7V are observed in the tracking signal. Fig. 16c shows the phase shift response measured and it shows high frequency chattering. Fig. 16a shows the measured results through oscilloscope

VI. CONCLUSION

This paper proposed novel adaptive artificial neural network based PI controller for the isolated bidirectional dual active bridge converter. At first, the mathematical model of the dual active bridge converter is approached, and the state space model is derived. Based on the state space model, the nonlinear controller for output voltage of DAB converter is derived. Then, another controller is derived which is based on artificial neural networks and is integrated with PI controller. All the derived controllers are extensively evaluated and tested on 150W prototype of DAB. The controllers are tested for three different types of variations, and their response of convergence to the reference is examined. Based on these tests, the novel artificial neural networks based PI controller gives better performance as compared to the others in regards of overshoot; undershoot, rise time and settling time. Furthermore, from the obtained results it is cleared that proposed controller shows creditable response for all types of variations and is robust to parameters mismatch.

REFERENCES

[1] E. Durán, J. M. Andújar, F. Segura, and A. J. Barragán, "A high-flexibility DC load for fuel cell and solar arrays power sources based on DC–DC converters," *Appl. Energy*, vol. 88, pp. 1690–1702, May 2011.

[2] M. Eccher, A. Salemi, S. Turrini, and R. S. Brusa, "Measurements of power transfer efficiency in CPV cell-array models using individual DC–DC converters," *Appl. Energy*, vol. 142, pp. 396–406, Mar. 2015.

[3] *Introduction of Electric Vehicle*, China Machine Press, Beijing, China, 2012, pp. 4–14.

[4] C. Wang, R. Xiong, H. He, X. Ding, and W. Shen, "Efficiency analysis of a bidirectional DC/DC converter in a hybrid energy storage system for plug-in hybrid electric vehicles," *Appl. Energy*, vol. 183, pp. 612–622, Dec. 2016.

[5] C.-C. Hua, C.-W. Chuang, C.-W. Wu, and D.-J. Chuang, "Design and implementation of a digital high-performance photovoltaic lighting system," in *Proc. ICIEA*, May 2007, pp. 2583–2588.

[6] N. Kasa, Y. Harada, T. Ida, and A. K. S. Bhat, "Zero-current transition converters for independent small scale power network system using lower power wind turbines," in *Proc. IEEE Int. Symp. Power Electron, Elect. Drives, Autom. Motion*, May 2006, pp. 1206–1210.

[7] S. Öztürk, P. Poşpoş, V. Utalay, A. Koç, M. Ermiş, and I. Çadırcı, "Operating principles and practical design aspects of all SiC DC/AC/DC converter for MPPT in grid-connected PV supplies," *Solar Energy*, vol. 176, pp. 380–394, Dec. 2018.

[8] C. Liu, X. Li, Y. Zhi, and G. Cai, "New breed of solid-state transformer mainly combing hybrid cascaded multilevel converter with resonant DC-DC converters," *Appl. Energy*, vol. 210, pp. 724–736, Jan. 2018.

[9] N. Ullah, M. I. Khattak, and W. Khan, "Fractional order fuzzy terminal sliding mode control of aerodynamics load simulator," *Proc. Inst. Mech. Eng., G, J. Aerosp. Eng.*, vol. 229, no. 14, pp. 2608–2619, 2015.

[10] T. F. Wu, Y. C. Chen, J. G. Yang, and C. L. Kuo, "Isolated bidirectional full-bridge DC–DC converter with a flyback snubber," *IEEE Trans Power Electron*, vol. 25, no. 7, pp. 1915–1922, Feb. 2010.

[11] H. Bai and C. Mi, "Eliminate reactive power and increase system efficiency of isolated bidirectional dual-active-bridge DC–DC converters using novel dual-phase-shift control," *IEEE Trans. Power Electron.*, vol. 23, no. 6, pp. 2905–2914, Nov. 2008.

[12] Z. Biao, Y. Qingguang, and S. Weixin, "Bi-directional full-bridge DC-DC converters with dual-phase-shifting control and its backflow power characteristic analysis," *Proc. CSEE*, vol. 32, no. 12, pp. 43–50, 2012.

[13] Y. A. Harrye, K. H. Ahmed, G. P. Adam, and A. A. Aboushady, "Comprehensive steady state analysis of bidirectional dual active bridge DC/DC converter using triple phase shift control," in *Proc. 3rd Int. Symp. Ind. Electron. (ISIE)*, Jun. 2014, pp. 437–442.

[14] M. Kim, M. Rosekeit, S.-K. Sul, and R. W. A. A. De Doncker, "A dual-phase-shift control strategy for dual-active-bridge DC-DC converter in wide voltage range," in *Proc. 8th Int. Conf. Power Electron.-ECCE Asia*, May/Jun. 2011, pp. 364–371.

[15] H. Zhang, X. Tong, and J. Yin, "Optimal triple-phase-shift controller design of isolated bidirectional DC-DC converter based on ant colony algorithm and BP neural network," in *Proc. 43rd Annu. Conf. Ind. Electron. Soc. (IECON)*, Beijing, China, Oct./Nov. 2017, pp. 8802–8807.

[16] W. L. Malan, D. M. Vilathgamuwa, G. Walker, D. J. Thrimawithana, and U. K. Madawala, "Modeling and control of a CLC resonant dual active bridge," in *Proc. Australas. Univ. Power Eng. Conf. (AUPEC)*, Perth, WA, Australia, Sep./Oct. 2014, pp. 1–6.

[17] S. Khade, A. Gaonkar, S. Weakey, R. Chavan, and R. Meshram, "Stability enhancement of rectifier and DAB stages of SST model using dynamic phasor based PI controller," in *Proc. IEEE 6th Int. Conf. Power Syst. (ICPS)*, New Delhi, India, Mar. 2016, pp. 1–6.

[18] G. G. Koch, S. S. Queiroz, C. Rech, R. C. L. F. Oliveira, R. A. Borges, E. S. Tognetti, and V. F. Montagner, "Design of a robust PI controller for a dual active bridge converter," in *Proc. 12th IEEE Int. Conf. Ind. Appl. (INDUSCON)*, Nov. 2016, pp. 1–6.

[19] M. Phattanasak, W. Kaewmanee, P. Thounthong, P. Sethakul, J.-P. Martin, S. Pierfederici, and B. Davat, "Flatness based control of a dual active bridge converter for DC microgrid," in *Proc. 39th Annu. Conf. IEEE Ind. Electron. Soc. (IECON)*, Vienna, Austria, Nov. 2013, pp. 7926–7931.

[20] B. Liu, Y. Zha, T. Zhang, and S. Chen, "Fuzzy logic control of dual active bridge in solid state transformer applications," in *Proc. Tsinghua Univ.-IET Elect. Eng. Acad. Forum*, Beijing, China, May 2016, pp. 1–4.

[21] S. Dutta, S. Bhattacharya, and M. Chandorkar, "A novel predictive phase shift controller for bidirectional isolated DC to DC converter for high power applications," in *Proc. IEEE Energy Convers. Congr. Expo. (ECCE)*, Raleigh, NC, USA, Sep. 2012, pp. 418–423.

[22] R. Zgheib and K. Al-Haddad, "Neural network controller to manage the power flow of a hybrid source for electric vehicles," in *Proc. IEEE Vehicle Power Propuls. Conf. (VPPC)*, Montreal, QC, Canada, Oct. 2015, pp. 1–6.

Z. Farooq et al.: Artificial Neural Network Based Adaptive Control of Single Phase DAB With Finite Time Disturbance Compensation

IEEE Access

[23] Y.-C. Jeung and D.-C. Lee, "Voltage and current regulations of bidirectional isolated dual-active-bridge DC–DC converters based on a double-integral sliding mode control," *IEEE Trans. Power Electron.*, vol. 34, no. 7, pp. 6937–6946, Jul. 2019. doi: 10.1109/TPEL.2018.2873834.

[24] Y.-C. Jeung, I.-C. Choi, and D.-C. Lee, "Robust voltage control of dual active bridge DC-DC converters using sliding mode control," in *Proc. IEEE 8th Int. Power Electron. Motion Control Conf. (IPEMC-ECCE Asia)*, Hefei, China, May 2016, pp. 629–634.

[25] J. M. Zurada, A. Malinowski, and P. Przestrzelski, "Modified Hebbian learning rule for single layer learning," in *Proc. IEEE Int. Symp. Circuits Syst.*, Chicago, IL, USA, vol. 4, May 1993, pp. 2407–2410. doi: 10.1109/ISCAS.1993.394249.

[26] D. Segaran, B. P. McGrath, and D. G. Holmes, "Adaptive dynamic control of a bi-directional DC-DC converter," in *Proc. IEEE Energy Convers. Congr. Expo.*, Sep. 2010, pp. 1442–1449.

[27] D. Segaran, D. G. Holmes, and B. P. McGrath, "Enhanced load step response for a bidirectional DC–DC converter," *IEEE Trans. Power Electron.*, vol. 28, no. 1, pp. 371–379, Jan. 2013.

[28] Y. Zhu, Z. Zhong, M. Basin, and D. Zhou, "A descriptor system approach to stability and stabilization of discrete-time switched PWA systems," *IEEE Trans. Autom. Control*, vol. 63, no. 10, pp. 3456–3463, Oct. 2018.

[29] L. Zhang, Y. Zhu, and W. X. Zheng, "State estimation of discrete-time switched neural networks with multiple communication channels," *IEEE Trans. Cybern.*, vol. 47, no. 4, pp. 1028–1040, Apr. 2017.

ZAHEER FAROOQ received the B.Sc. and M.Sc. degrees in electrical engineering from the University of Science and Technology, Peshawar, Pakistan, in 2003 and 2009, respectively. He is currently pursuing the Ph.D. degree with the CECOS University of IT and Emerging Sciences, Peshawar, Pakistan, where he is currently an Assistant Professor. His current research interests include motor control and drives, renewable energy, and control of DC/DC power converters.

TAIMUR ZAMAN received the B.Sc. and M.Sc. degrees from COMSTAS Islamabad and the CECOS University of IT and Emerging Sciences, Peshawar, Pakistan, in 2015 and 2018, respectively. He is currently a Research Assistant with the Department of Electrical Engineering, CECOS University of IT and Emerging Sciences. His research interests include nonlinear control systems, integer and fractional-order modeling of dynamic systems, motor control and drives, renewable energy, and power converters.

MUHAMMAD AMIR KHAN received the B.Sc. degree in electronics engineering from International Islamic University, Islamabad, Pakistan, in 2018. He is currently a Research Assistant with the Department of Electrical Engineering, CECOS University of IT and Emerging Sciences, Peshawar, Pakistan. His research interests include motor control and drives, renewable energy, and control of dc–dc power converters.

NASIMULLAH received the Ph.D. degree in mechatronic engineering from Beihang University, Beijing, China, in 2013. From 2006 to 2010, he was a Senior Design Engineer with IICS, Pakistan. He is currently an Associate Professor of electrical engineering with the CECOS University of IT and Emerging Sciences, Peshawar, Pakistan. His research interests include renewable energy, flight control systems, integer and fractional order modeling of dynamic systems, integer/fractional order adaptive robust control methods, fuzzy/NN, hydraulic and electrical servos, epidemic, and vaccination control strategies.

S. M. MUYEEN (S'03–M'08–SM'12) received the B.Sc. Eng. degree from the Rajshahi University of Engineering and Technology (RUET), formerly known as Rajshahi Institute of Technology, Bangladesh, in 2000, and the M.Eng. and Ph.D. degrees from the Kitami Institute of Technology, Japan, in 2005 and 2008, respectively, all in electrical and electronic engineering. He is currently an Associate Professor with the School of Electrical Engineering Computing and Mathematical Sciences, Curtin University, Australia. He has published more than 200 articles in different journals and international conferences. He has published six books as an Author or an Editor. His research interests include power system stability and control, electrical machine, FACTS, energy storage system (ESS), renewable energy, and HVDC systems. He is also a Fellow of Engineers Australia. He has been a Keynote Speaker and an Invited Speaker at many international conferences, workshops, and universities. He has been serving as an Editor/Associate Editor for many prestigious journals of IEEE, IET, and other publishers, including IEEE Transactions on Sustainable Energy, IEEE Power Engineering Letters, *IET Renewable Power Generation*, and *IET Generation, Transmission & Distribution*.

ASIER IBEAS was born in Bilbao, Spain, in 1977. He received the M.Sc. degree in applied physics and the Ph.D. degree in automatic control from the University of the Basque Country, Spain, in 2000 and 2006, respectively. He is currently an Associate Professor of control systems with the Autonomous University of Barcelona, Spain. He is also a Full Professor with the Catalan Agency for Quality in Higher Education. He has authored over 130 contributions in international journals and conferences. He has supervised and is currently advising several doctoral theses and has participated in numerous research projects funded by regional and national agencies. His research interests include time-delayed systems, robust adaptive control, applications of artificial intelligence to control systems design, and nonconventional applications of control, such as to epidemic systems, supply chain management, and numerical systems.

• • •